J Mater Sci (2011) 46:1474–1486
DOI 10.1007/s10853-010-4949-7

New insights in photo-patterned sol–gel-derived TiO_2 films

S. Briche · Z. Tebby · D. Riassetto · M. Messaoud · E. Gamet · E. Pernot · H. Roussel · O. Dellea · Y. Jourlin · M. Langlet

Received: 29 June 2010 / Accepted: 22 September 2010 / Published online: 16 October 2010

Abstract Specific sol–gel formulations and protocols have been adapted to the fine patterning of TiO_2 films using a very simplified UVA three-step lithography method. Mechanisms occurring during the photo-patterning procedure and a post-patterning thermal treatment have been studied by Fourier transform infrared spectroscopy, atomic force microscopy, X-ray diffraction, and ellipsometry. Discussions are proposed to support the influence of the photo-patterning procedure and post-patterning treatment on the shape and the dimension of so-formed microstructures. Original additional functionalities arising from such structures are also presented.

Introduction

Over the past decades, titanium oxide films have largely been studied for a great number of applications, including photocatalytic surfaces, photovoltaic cells, coatings for optics, or in waveguides for integrated optical devices, because of numerous inherent properties such as photo-induced properties, high refractive index, wide optical band gap, or weak absorption in the visible and near-infrared spectral regions [1, 2]. In this context, TiO_2 films should play an important role in micro- and nano-technologies, which introduces the interest to study the possibility of carrying out micrometric or sub-micrometric structuration in such films. A very wide range of lithography methods have been proposed in the literature to create fine nano- or micrometric patterns on various supports [3–16]. However, these methods often remain delicate to implement because they generally require very sophisticated heavy equipments and/or complex procedures.

In recent years, several works have been devoted to the direct photo-patterning of sol–gel-derived oxide films [17–21]. This photo-patterning method is based on a chemical modification (chelation) of metal alkoxide precursors with a suitable organic ligand, and a subsequent localized exposure of derived gel films to ultraviolet (UV) light. By inducing a photolytic decomposition of the chelate, UV light promotes a drastic increase in the chemical stability of irradiated areas in the gel film, which allows a selective washing of non-irradiated areas and the direct formation of fine patterned structures, i.e. a negative resist-like behaviour. This patterning method opens the route to new low-cost and simplified protocols in different applications fields due to its powerful control on the structure and the properties of photo-imprinted films and compatibility with substrates of large areas and/or complex shapes. For instance, this method has been proposed for the UVA or UVB photo-imprinting of fine surface-relief gratings in sol–gel-derived Al_2O_3, ZrO_2 or PLZT films [20]. Benzoylacetone (BzAc) is generally proposed as a ligand when UVA photo-patterning is implemented [19]. Phenyl groups of this ligand extend absorption of the derived metal complex over the whole UVA range. However, in the case

S. Briche · D. Riassetto · M. Messaoud · E. Pernot · H. Roussel · M. Langlet (✉)
LMGP, Grenoble Institute of Technology-Minatec, 3 Parvis Louis Néel, 38016 Grenoble, France
e-mail: Michel.Langlet@grenoble-inp.fr

Z. Tebby · O. Dellea
PF D2 M/CEA LITEN, 18 Rue Benoît Lauras, Bât. G, 42000 St-Etienne, France

E. Gamet · Y. Jourlin
LabHC, Université Jean Monnet, 18 Rue Benoît Lauras, Bât. F, 42000 St-Etienne, France

of BzAc-based sol–gel TiO_2 films, it was not so easy to form uniform gratings, because the solubility contrast between irradiated and non-irradiated areas was insufficient [18]. Alternative ligands have recently been proposed to form micrometric or sub-micrometric patterns in sol–gel TiO_2 films, such as methacrylic acid for a deep-UV (193 nm) laser printing [17], or 1-(2-hydroxyphenyl)-3-phenyl-2-propen-1-one to create fine patterns through a mask using a high pressure mercury lamp emitting in the 250–450-nm range [21]. However, the authors provide very few experimental data and information on involved mechanisms. Actually, this remark prevails for most studies devoted to the patterning of TiO_2 films using such a simplified method. Thus, additional researches still remain necessary to extend the range of available light sources compatible with the patterning of sol–gel TiO_2 films, for instance traditional UVA laser diodes, and to better understand and optimize involved mechanisms.

In this study, we have performed new investigations on the fine UVA photo-patterning of TiO_2 films deposited from an alcoholic BzAc-modified sol. Specific sol formulations have been developed, which allow an enhanced chemical solubility contrast between irradiated and non-irradiated regions and enable a flexible patterning of micrometric or sub-micrometric structures using simple mask or laser lithography methods. Some mechanisms and derived structuration features are discussed in relation to irradiation and thermal post-treatment conditions, on the basis of Fourier transform infrared (FTIR) spectroscopy, ellipsometry, X-ray diffraction (XRD), and atomic force microscopy (AFM) measurements. We also present some original functionalities arising from the photocatalytic activity and chemical reactivity of so-formed TiO_2 structures.

Experimental

Formulation of a mixed TIPT solution

Figure 1 shows a flow chart for the preparation of photosensitive TiO_2 gel films compatible with a fine patterning process. To optimize photo-patternable films, a mixture of two sols of different reactivities has been prepared. The first sol (sol 1) exhibits a very weak chemical reactivity due to chelation of the alkoxide by BzAc. Accordingly, derived films were observed to totally dewet the substrate during the liquid–solid transition (sol–gel transformation), owing to the insufficient development of a stiff inorganic network able to counteract surface tension that develops during this transition. The second sol (sol 2) was adapted from a protocol previously optimized in our lab, which yielded sols very stable in bottle but strongly reactive once deposited in the form of a liquid film [22]. Even in the absence of any post-treatment, gel films deposited from such a sol can hardly be leached with alcohol.

Sol 1 was prepared by reacting tetraisopropylorthotitanate (TIPT from Fluka) with BzAc (from Aldrich) in methyl alcohol (MeOH from Prolabo). The TIPT/BzAc/MeOH molar composition was 1/0.91/20.4. Sol 2 was obtained by mixing TIPT with deionized water, hydrochloric acid (HCl from Roth), and butyl alcohol (BuOH from Alfa Aesar) as a solvent. The TIPT concentration in the solution was 0.4 M, and the TIPT/H_2O/HCl/BuOH molar composition was 1/0.82/0.13/23.9. For this sol, the theoretical pH value calculated from the amount of HCl was 1.27. The sol was aged at room temperature for 2 days before use, after what it could be employed for several months in reproducible conditions. Finally, the photosensitive solution was prepared by mixing sols 1 and 2 to

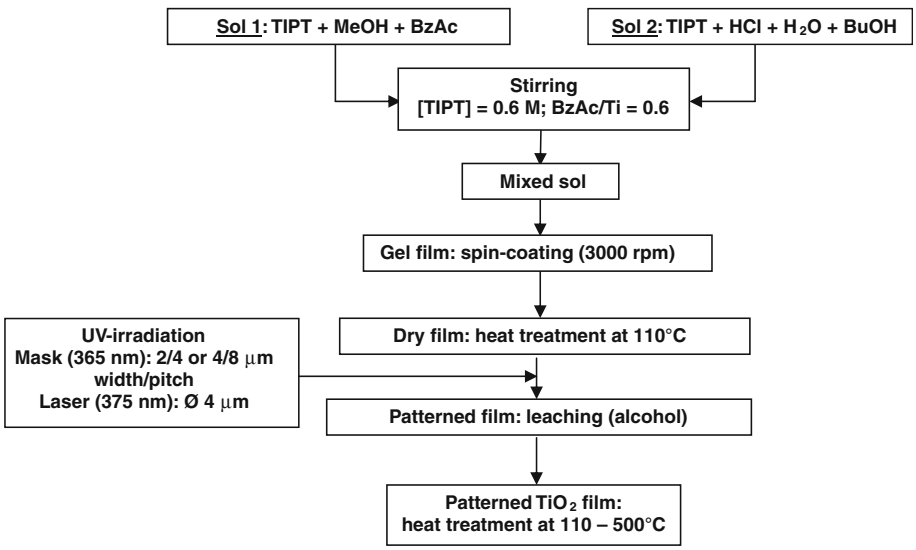

Fig. 1 Flow chart for the preparation of photo-patterned TiO_2 films deposited from a Ti–BzAc sol

obtain a final sol with a TIPT concentration of 0.6 M and a BzAc/TIPT molar ratio of 0.6. These conditions were fixed according to preliminary works yielding an optimized film quality (homogeneity, optical grade).

Formation of TiO_2 films

Films were deposited at room temperature, on (100) silicon wafers (from Siltronix) or glass plates, by spin-coating on 3×3 cm^2 samples using a Suss Microtec RC8 apparatus. Prior to deposition, the substrates previously stored in deionised water were then cleaned with ethanol and dried with air spray. For each deposition, 300 μL of sol were spread on the substrate rotated at 3,000 rpm for 1 s. After liquid film deposition, the solvent slowly evaporated and a gel film formed at ambient atmosphere through the well-known sol–gel polymerization route. The as-deposited gel films could then be photo-patterned using the three-step procedure described below. The effects of a heat-treatment in air were also tested, on films photo-patterned or not, for a duration of 15 min in a 110–500 °C thermal range. Film samples were directly introduced in the furnace pre-heated at a fixed temperature. As will be shown below, heat-treatment at a sufficiently high temperature promoted crystallization of the TiO_2 anatase phase. In some cases, a multilayer deposition procedure was adopted to adjust the film thickness. Additional elaboration conditions will be described in 'Result'.

Photo-patterning of gel films

Photo-patterning of gel films was tested in two ways. Routine tests were performed using a glass-supported chromium mask constituted of periodic gratings of 2/4 or 4/8-μm width/pitch. For that purpose, a mercury lamp (HPLN-50 from Philips) was used, which mainly emitted at a 365-nm wavelength (light power density of ca. 3 mW/cm^2), and the sample was illuminated through hard contact with the mask. Photo-patterning tests were also performed using a laser printing commercial device (Dilase 750) equipped with a laser diode emitting at 375 nm. A devoted optical arm enables to shape and focus the laser beam on the sample to be patterned. The focalized laser beam has a circular symmetry and a constant diameter whose lowest value is 4 μm. Moreover, the optical arm ensures a homogeneous field with a field depth superior to 10 μm. Focalization of the laser beam is achieved through a lens mounted on a micrometric screw, which allows a precise positioning in respect to the sample to be patterned. Position of the lens is defined with respect to an arbitrary zero value. The sample is dynamically illuminated during its displacement under the laser beam using a computer-driven micro-displacement system. In this study, the light power at the sample surface was fixed at 100 μW. The writing speed, i.e. displacement speed of the sample under the laser beam, was 0.001 mm/s. Strips of 2-mm length were formed at different intervals using a constant speed and lens position. After writing each strip, the lens position was modified by 20-μm steps, in an arbitrary 580–700 μm position range, to define best focalization conditions of the laser beam. A three-step procedure, which will be discussed in next sections, was implemented to photo-pattern Ti-BzAc films. Gel films were first dried for 2 min or 2 h at 110 °C, then exposed to UVA light through a mask or using a laser diode, and finally post-treated for 8 min at 110 °C. The films were then rapidly washed with absolute ethanol to etch non-irradiated areas before eventual subsequent heat-treatment.

Characterization methods

UV/visible transmission spectra of films deposited on glass were measured in the 200–1100-nm range using a Jasco V-530 spectrophotometer. All other characterizations were performed on films deposited on silicon. FTIR spectra were acquired in transmission configuration in the 4000–275 cm^{-1} spectral range using a Bio-Rad FTS-165 spectrometer. Spectra of 300 scans were recorded in room atmosphere under dry air sweeping with a resolution of 4 cm^{-1}. The spectra were analysed after subtraction of the bare silicon substrate spectrum. XRD measurements were performed in grazing incidence using a BRUKER-D8-Advance diffractometer with a 0.27° incidence angle and a Cu Kα X-ray source ($\lambda = 0.15418$ nm). Refractive indices and thicknesses of the films were measured by monochromatic ellipsometry using a Gaertner L116B apparatus operated at a 633-nm wavelength. The profiles of photo-patterned strips were analysed by AFM using a Digital Instrument Nanoscope microscope in tapping mode. RMS roughness values of photo-patterned strips were deduced from AFM studies by spectral analysis performed on several 1-μm^2 areas of the strips. Morphology features were also analysed by field emission gun scanning electron microscopy (FEG-SEM) using a HITACHI S-4500 microscope operated at 5 kV. Water contact angle measurements (sessile droplet method; water pH 5.7) were performed at room temperature using a drop shape analysis system (Kruss DSA 10 MK2) connected with a video camera. The sample was sprayed with a jet pure gas (Presi) before measurement. An average contact angle was determined from values measured on left and right sides of four droplets of 0.5 μL deposited on different areas of the film surface.

Results and discussion

General features

Photosensitive sols studied in this study were based on the complexation of TIPT with BzAc. Roughly speaking, BzAc is a β-diketone which exhibits two C=O double bounds attached to a phenyl ring. The reaction of BzAc with metal alkoxides promotes the opening of these C=O double bounds and a part of the alkoxy groups are readily substituted with β-diketonato ligands to form chelate rings [18]. A chemical structure of the resulting complex is schematically illustrated in the inset of Fig. 2. Such a complexation with β-diketones is frequently performed to reduce or suppress the reactivity of metal alkoxides, so that gel films formed from such complexes can easily be leached through simple washing with alcohols [18–20]. Figure 2 shows the typical FTIR spectrum of a gel film deposited from the BzAc-derived mixed sol (sol 1 + sol 2) studied in this study. No post-deposition drying treatment was performed for this film. As illustrated in Fig. 2, essential spectral features appear in the 2000–275 cm^{-1} range. Additional features observed in the 3000–2700 cm^{-1} range mainly depicted C–H bonds attributed to residual solvent in the gel films (not illustrated here). The IR spectrum illustrated in Fig. 2 exhibits numerous bands which can commonly depict several components arising from our mixed sol. An exhaustive assignment of these bands is obviously out of the topics of this work. Roughly speaking, three spectral regions of interest can be appreciated, which are indicated in Fig. 2. In the low wavenumber range, a structured broad band extending from 900 to 275 cm^{-1} depicts the efficient development of an oxo-polymer through sol–gel reactions [23]. As explained before, sol 1 component of the mixed sol exhibits very weak sol–gel reactivity. Thus, this oxo-polymer essentially arises from the sol 2 component. In a second region, a poorly resolved multi-component band extending from 1150 to 1050 cm^{-1} is essentially attributed to residual butanol used as solvent in sol 2 [24]. It indicates that, owing to its weak volatility, this solvent remains partially present in the film in the absence of any drying treatment, which was confirmed by bands observed in the 3000–2700 cm^{-1} range. A third region of interest, in the 1600–1480 cm^{-1} spectral range, essentially depicts main IR bands of the Ti–BzAc complex [19]. Absorption bands related to the chelate rings are observed at 1595 and 1520 cm^{-1}, while phenyl group stretching vibrations are evidenced by bands at 1560 and 1485 cm^{-1}. Residual solvent or non-reacted alkoxy groups of TIPT can also partially contribute to the bands observed in this later region. All other bands non-mentioned above arise from organic bonds, which can commonly depict the presence of organic solvent, non-reacted alkoxy groups, or additional bonds of the Ti–BzAc complex. To summarize, the film illustrated in Fig. 2 is constituted of an inorganic oxide network (oxo-polymer derived from sol 2) which incorporates residual organic species including chelating ones. These latter species make the Ti–BzAc complex particularly soluble in alcohols. Accordingly, films deposited from the mixed sols without any additional post-deposition treatment could easily be leached through rapid ethanol washing. Washing yields the dilution of soluble species, which in turn probably induces a destabilisation and subsequent leaching of the oxide network.

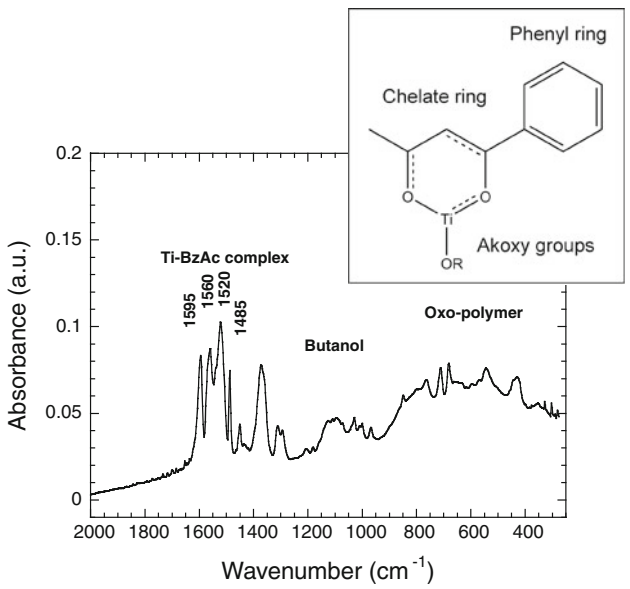

Fig. 2 IR spectrum of a gel film deposited from a Ti–BzAc sol. Main spectral regions discussed in the text are indicated and main chelate and phenyl bands of the Ti–BzAc complex are indexed according to the chemical structure of this complex schematically illustrated in the *inset*

As indicated in the experimental section, the mixed sol formulation was preliminary optimized to produce TiO_2 films of optical quality. This feature is illustrated in Fig. 3, which shows transmission spectra in the UV/visible spectral range for a bare glass substrate and for a TiO_2 film deposited on glass and subsequently heat-treated at 500 °C. The film thickness was adjusted to around 200 nm using a multilayer procedure. The film spectrum illustrated in this figure exhibits pronounced interference fringes resulting from multi-reflections at the film–air and film–substrate interfaces. According to interferential optics principles, for a transparent thin film of high refractive index deposited on a transparent substrate of lower refractive index, transmission minima are obtained when the optical thickness of the film corresponds to odd multiples of the quarter-wavelength, i.e. when the mismatch of refractive indices between substrate and film induces a maximum of reflection. For the film spectrum illustrated in Fig. 3, two transmission minima appear to be located at around 430

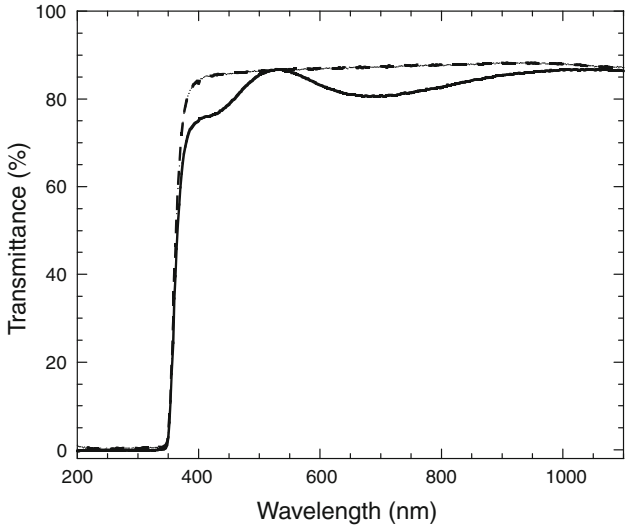

Fig. 3 Visible transmittance spectra of a bare glass substrate (- - -) and glass coated with a multilayer TiO_2 film deposited from a Ti-BzAc sol (—)

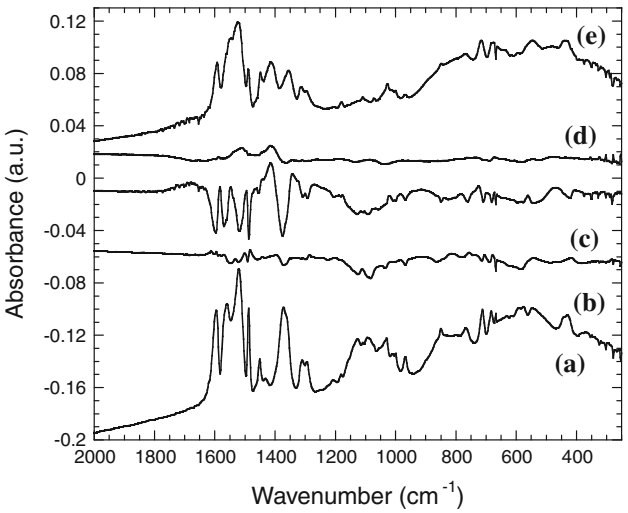

Fig. 4 IR spectra of a gel film during the three-step lithographic procedure (without mask). Spectra of (*a*) and (*e*) correspond to the initial and final gel spectra, respectively. Intermediary differential spectra depict evolutions occurring during a pre-drying treatment at 110 °C for 2 min (*b*), an UVA exposure for 1 h (*c*), and a final heat-treatment at 110 °C for 8 min (*d*)

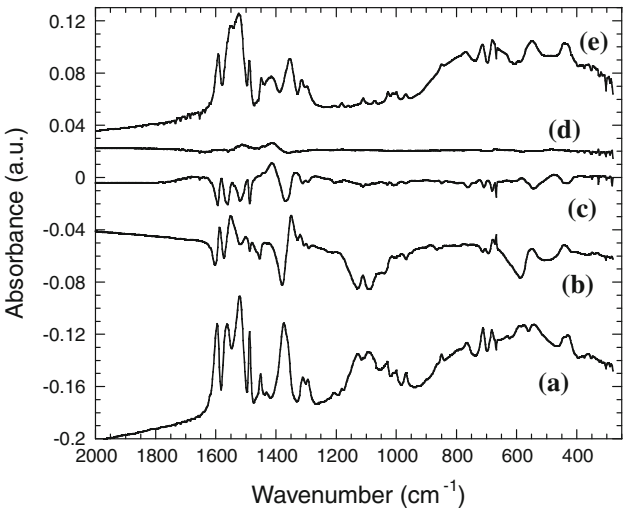

Fig. 5 IR spectra of a gel film during the three-step lithographic procedure (without mask). Spectra of (*a*) and (*e*) correspond to the initial and final gel spectra, respectively. Intermediary differential spectra depict evolutions occurring during a pre-drying treatment at 110 °C for 2 h (*b*), an UVA exposure for 1 h (*c*), and a final heat-treatment at 110 °C for 8 min (*d*)

and 700 nm. Spectral features below 400 nm can also partly be influenced by the energy band gap (*Eg*) of titanium oxide (for the anatase phase of TiO_2, $Eg = 3.2\ \text{eV} \Rightarrow \lambda = 380\ \text{nm}$). Below 350 nm, no transmission could be measured because of the glass substrate absorption. According to same optical principles, transmission maxima are obtained when the optical thickness of the film corresponds to even multiples of the quarter-wavelength. Theoretically, at these wavelengths the film is optically non-active, i.e. for an optical quality film, the transmission values should fit the bare substrate transmission. For the film spectrum illustrated in Fig. 3, two transmission maxima appear to be located at around 520 and 1070 nm. These transmission maxima closely fit the transmission level measured for the bare substrate. This feature clearly evidences the excellent optical quality (transparency) of our films, i.e. the absence of optical (diffusion, absorption) losses in the visible spectral range.

Chemical mechanisms involved in the photo-patterning procedure

Figures 4 and 5 show IR spectra of gel films preliminarily dried for 2 min and 2 h at 110 °C, respectively, before UVA exposure for 1 h using a mercury lamp (without mask), and subsequent heat-treatment for 8 min at 110 °C. Spectra of Figs. 4a and 5a correspond to the non-dried gel films, and logically exhibit very similar aspects. Differential spectra of Figs. 4 and 5b–d illustrate chemical modifications occurring during the three steps of the patterning procedure. Spectra of Figs. 4e and 5e correspond to the final film spectrum. Negative bands, observed at 1380, 1130, and 1090 cm^{-1}, in the differential spectra of Figs. 4b and 5b, clearly depict the evaporation of residual butanol during the pre-drying treatment at 110 °C. This evaporation is logically much more pronounced after a long pre-drying treatment (Fig. 5b). Actually, the butanol broad band located between 1150 and 1050 cm^{-1} could no longer be observed after drying for 2 h, which was also confirmed by the extinction of corresponding C–H bands in the high

wavenumber range (not illustrated here). The differential spectrum of Fig. 5b indicates that this efficient butanol evaporation is accompanied by additional features. In particular, successive negative and positive bands observed between 1600 and 1300 cm^{-1} depict some intensity reduction and/or shifting of bands associated to the Ti–BzAc complex (chelate, phenyl, and other bonds). Similar features can hardly be appreciated after a short pre-drying treatment (Fig. 4b). However, such chemical modifications have minor consequences, since gel films dried for 2 min and 2 h exhibited comparable solubility to rapid ethanol washing, similarly to non-dried films.

The negative band located between 1150 and 1050 cm^{-1} in the differential spectrum of Fig. 4c shows that evaporation of residual butanol, still present after a short pre-drying treatment, continues to take place during the UVA irradiation step. In contrast, the absence of any modification in this region for the spectrum of Fig. 5c definitively proves that butanol has been efficiently evaporated after a long pre-drying treatment. Besides, differential spectra of Figs. 4c and 5c illustrate a partial photolytic decomposition of the Ti–BzAc complex. Negative bands observed at 1595 and 1520 cm^{-1} depict a partial decomposition of the chelate rings induced by UV exposure [18–20]. This decomposition is also accompanied by negative bands of phenyl groups, at 1560 and 1485 cm^{-1}, and other negative bands which presumably correspond to a partial disappearance of additional organic groups associated to the complex. Intensities of negative bands observed in spectra of Figs. 4c and 5c show that this photolytic decomposition is more pronounced when the film has been pre-dried for a short time. It suggests that, either the presence of residual butanol favours a more efficient photolytic process, or modifications of the Ti-BzAc induced by a long pre-drying treatment (Fig. 5b) reduce this photolytic efficiency. The partial photolytic decomposition of easily leachable chelated species is expected to promote an increased chemical stability of irradiated gel films [18–20]. Moreover, it has been reported that only a few chelate rings are required to be broken to produce such stabilization [19]. Accordingly, despite differences observed between spectra of Figs. 4c and 5c, films pre-dried for a short or long duration and subsequently exposed to UV light exhibited similar stability to a rapid ethanol washing. It should be noted that this stabilization is only due to the partial chelate decomposition, since differential spectra of Figs. 4c and 5c do not show any growth of the oxo-polymer broad band (900–275 cm^{-1}), which would eventually indicate a complementary development of the oxide network through additional sol–gel reactions. It is inferred that the degree of oxo-polymerization induced by the strong reactivity of sol 2 has reached a maximum that cannot be improved through a complementary room temperature (photo-assisted) treatment. However, we also observed that a more intensive washing slightly degraded the irradiated film quality. For this reason, a post-irradiation heat-treatment for 8 min at 110 °C was adopted, which enhanced the stability to intensive ethanol washing.

Effects related to this post-treatment are illustrated in Fig. 4d and 5d, which only show the appearance of positive bands at 1520 and 1410 cm^{-1}. These bands probably correspond to titanium carbonate species [25]. They were also observed after annealing BzAc-modified gel films in a 300–400 °C thermal range and appeared as intermediary species in the film oxidation and subsequent crystallization at higher temperature (not illustrated here). Photo-induced modifications illustrated in spectra of Figs. 4c and 5c probably produce volatile species, which can desorb the film sample [19]. However, some of these species can also remain incorporated in the film and may eventually participate to its partial residual solubility. It is thus believed that formation of carbonated species illustrated in Figs. 4d and 5d arises from the oxidation of residual photolytic decomposition products still incorporated in the film. Accordingly, the intensity of carbonate bands is quite stronger in the case of a film pre-dried for a short duration (Fig. 4d), which can be related to a more efficient photolytic process illustrated in Fig. 4c yielding a greater amount of species prone to be oxidized. Finally, since titanium carbonate species are inherently non-soluble in ethanol, it can in turn explain a reinforced stability of post-treated films to intensive ethanol washing. Figures 4e and 5e show that the final film spectra exhibit certain differences, which arise from the different mechanisms involved during the three-step procedure in relation to the pre-drying treatment duration. In particular, some traces of butanol could still be detected (low- and high-wavenumber ranges) for a film pre-dried for a short duration. However, despite such differences, both kinds of films exhibited similar resistance to intensive ethanol washing.

To summarize, this study enabled us to induce a strong solubility contrast between irradiated and non-irradiated gel films, owing to (i) the solubility of chelated species arising from sol 1, and (ii) the photolytic decomposition of these species together with the efficient development of a stable oxo-polymer arising from sol 2. This solubility contrast could be optimized using a three-step photo-patterning procedure consisting of a pre-drying treatment, an UV exposure, and a subsequent post-treatment. As will be discussed in next sections, the pre-drying treatment plays a particular role in structures formed from such a three-step photo-patterning procedure.

Photo-patterned films

In order to assess the effects of an enhanced solubility contrast on the fine patterning of sol–gel TiO_2 films,

preliminary tests were performed using a photolithographic mask transfer method under UVA light emitted by a mercury lamp. Figure 6a shows the typical AFM image of a gel film dried for 2 h at 110 °C before irradiation for 1 h through a 2/4-μm width/pitch periodic grating, subsequent heat-treatment for 8 min at 110 °C, and ethanol washing. This image illustrates linear strips with an excellent width and height regularity. Height of these strips is about 300 nm, which closely corresponds to the thickness measured by ellipsometry for a film heat-treated in similar conditions. These features indicate that non-irradiated areas of the photo-patterned film illustrated in Fig. 6a have totally been removed by ethanol washing. Very weak RMS roughness values of around 0.8 ± 0.05 nm were also measured in several areas of the strips, which confirmed the good quality and homogeneity of patterns formed using our simplified lithography method. However, it should be mentioned that a selective post-irradiation washing could be performed only after a rather long UV irradiation of 1 h. Photo-patterned strips were partially leached when using shorter irradiations conditions, which illustrated that the fine patterning of our films required a rather long chelate photo-decomposition process. This observation indicates that further studies are still required to optimize our fine patterning procedure. As mentioned above, the mixed sol formulation used in this study was preliminarily fixed with respect to film optical quality criteria. However, it is possible that the amount of BzAc, which determines the facility of the non-irradiated film to be leached, is still too strong. A sufficient photolytic decomposition of the complex and efficient stabilization of the irradiated areas should thus require an important UV dose. In the future, new studies will be conducted to reduce the UV dose. New formulation with weaker BzAc amounts can be envisaged. An UV pre-treatment without mask can also permit a partial and controlled photolytic decomposition of the BzAc complex in excess.

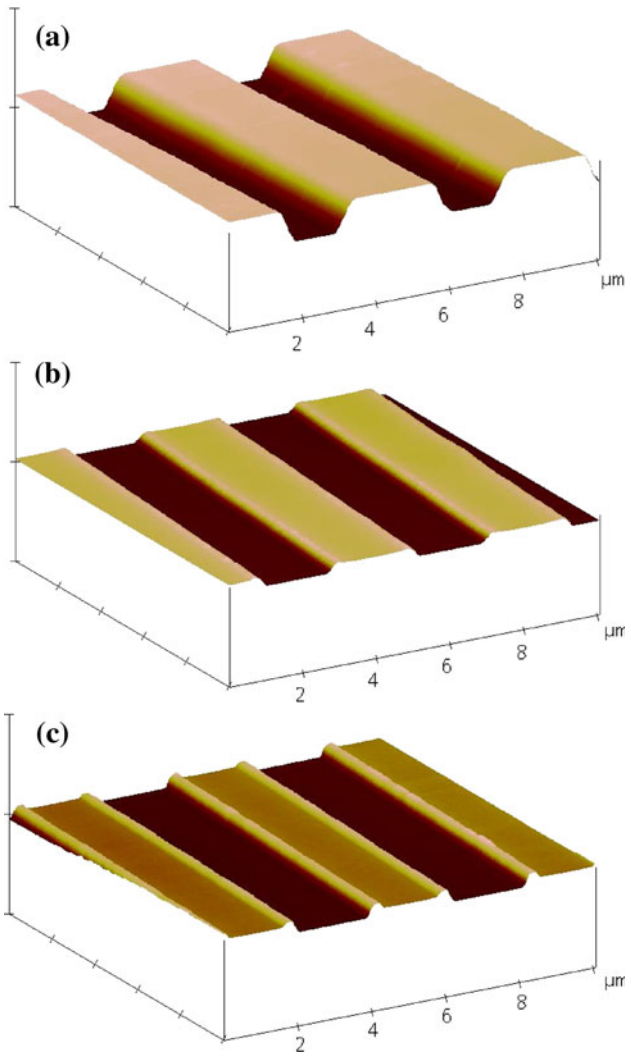

Fig. 6 AFM images of strip profiles formed through a 2/4-μm width/pitch mask on a film pre-dried for 2 h at 110 °C before (**a**) and after post-patterning treatment for 15 min at 500 °C (**b**), and for a film pre-dried for 2 min at 110 °C and submitted to a post-patterning treatment at 500 °C for 15 min (**c**). Full scales in vertical and horizontal dimensions are 1 and 10 μm, respectively

Figure 6a also shows that strip edges are not vertical. The edge slope, which was measured to be ca. 35° in the example of Fig. 6a, can partly be due to diffraction effects through the mask motifs since, according to the photo-patterned strip dimensions and use of a mercury lamp, we are probably close to the exposure limits. Artefacts caused by the conic shape of the tip used for AFM measurements are excluded, since we have previously shown that the shape and dimension of this tip cannot induce slopes inferior to 55° [26]. Generally speaking, similar regularities and qualities of photo-patterned profiles were also obtained for gel films pre-dried for 2 min at 110 °C. However, as illustrated in Fig. 7, the pre-treatment duration induces some differences in the profile shapes of so-formed structures. This figure first shows that photo-patterned structures exhibit heights of 350 and 300 nm in the case of films pre-dried for 2 min and 2 h at 110 °C, respectively. It suggests that increasing the pre-treatment duration promotes a more efficient densification of resulting photo-patterned structures. Besides, Fig. 7 shows that, while widths at the bottom of photo-patterned structures are rather comparable, a shorter pre-drying treatment induces a stronger width reduction at the top of photo-patterned structures. This feature suggests some influence of the pre-drying treatment on the solubility contrasts yielding micrometric structures in relation to differences in mechanisms illustrated in Figs. 4 and 5.

These results were then transposed to the fine patterning of TiO_2 films using an UVA laser diode. A laser system allows a very flexible control of the UV dose through the

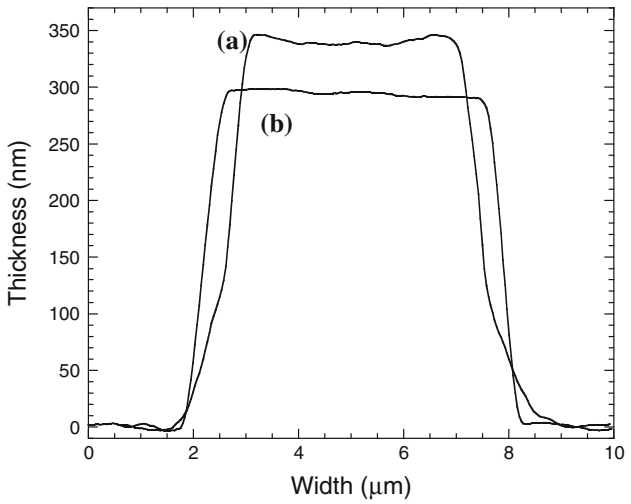

Fig. 7 AFM analysis of strip profiles formed through a 4/8-μm width/pitch mask on a gel film pre-dried for 2 min at 110 °C (*a*) and 2 h at 110 °C (*b*). No heat-treatment was performed after the photo-pattering procedure

variation of multiple parameters (laser power, imprinting speed, laser lens position), which in turn enables to precisely monitor the pattern dimensions on large-scale substrates. Moreover, a laser diode provides an easy and low-cost way to produce a fine patterning. Laser tests were performed at various lens positions on gel films preliminarily dried for 2 min at 110 °C. As illustrated in Fig. 8, a variation of this lens position from 580 to 700 μm leads to a reduction of the photo-imprinted strip width, measured at mid-height of photo-patterned structures, from 17 to about 3.5–4 μm. This latter dimension fairly corresponds to the diameter of the laser beam (4 μm), which indicates an optimization of focalization conditions, and it is obtained

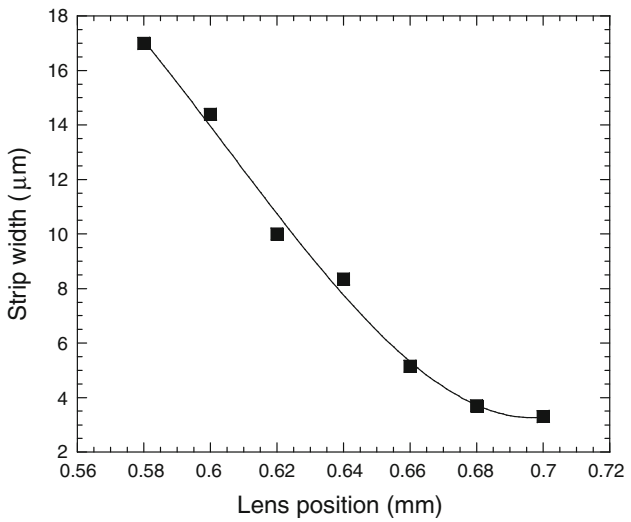

Fig. 8 Influence of the laser lens position on the width of strips imprinted on a TiO_2 film with an imprinting speed of 0.001 mm/s

for a rather large focalisation tolerance of 20 μm, which depicts that our laser device ensures a homogeneous field within an important depth. A structure regularity similar to that illustrated in Fig. 6a was obtained (not illustrated here), which indicated that our experimental procedure was well adapted to a fine patterning using a laser diode system. However, this pattern quality could only be obtained for a slow imprinting speed of 0.001 mm/s, which corroborated long irradiation durations required to finely pattern gel films through our previous mask procedure. Moreover, non-vertical strip edges were also formed through laser imprinting, which showed that this feature was not due only to diffraction effects through a mask and should be the object of further studies.

Thermal treatment effects

Figures 9 and 10 present structure profiles analysed by AFM for films pre-dried for 2 min and 2 h at 110 °C, respectively, before irradiation for 1 h through a 4/8-μm width/pitch mask, heat-treatment for 8 min at 110 °C, ethanol washing, and subsequent cumulative heat-treatments for 15 min at increasing temperatures in the 200–500 °C thermal range. AFM images of microstructures, formed through a 2/4 μm width/pitch mask and subsequently post-treated at 500 °C, are also presented in Fig. 6b and c for films pre-dried for 2 h and 2 min at 110 °C, respectively. Figures 9 and 10 show that increasing the post-treatment temperature yields a considerable reduction of the photo-patterned structure thickness. Heights at the profile centre are measured to be 300 and 250 nm after a post-treatment at 200 °C for films initially pre-treated for 2 min and 2 h at 110 °C, respectively. This height difference corroborates that illustrated in Fig. 7 and confirms that a longer pre-treatment duration promotes the densification of photo-patterned structures. Width at the top of structures arising from a shorter pre-drying treatment is also observed to be smaller than in the case of a longer pre-treatment, which also corroborates data illustrated in Fig. 7. Figures 9 and 10 show that for both the durations of pre-treatment, height at the profile centre decreases down to ca. 80 nm when increasing the post-treatment temperature up to 500 °C. This feature illustrates thermo-induced densification effects. Ellipsometry measurements performed on non-patterned films confirmed such effects, showing that the film refractive index increased from 1.7 to 2.3 when increasing the heat-treatment temperature from 110 to 500 °C. These variations indicate that (i) films heat-treated at low temperature are rather porous owing to the inherent structure of sol–gel-derived materials, and (ii) thermo-induced densification efficiently occurs at higher temperatures since the refractive index (2.3) of films annealed at 500 °C approaches the value of bulk TiO_2 (2.5

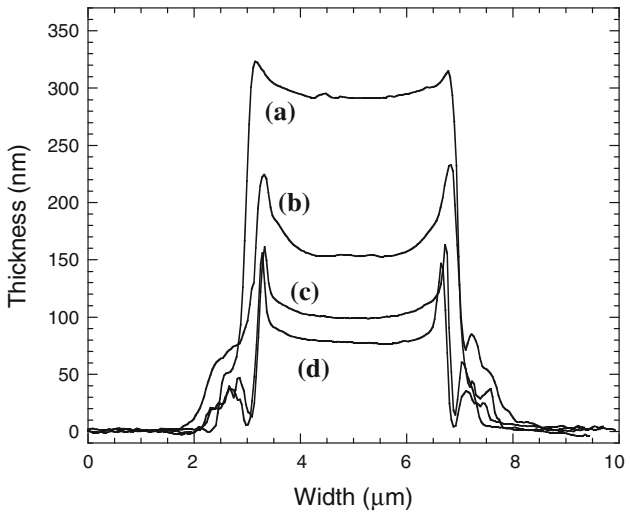

Fig. 9 AFM analysis of strip profiles formed through a 4/8-μm width/pitch mask on a gel film pre-dried for 2 min at 110 °C and submitted to post-patterning cumulative heat-treatments for 15 min at 200 (*a*), 300 (*b*), 400 (*c*), and 500 °C (*d*)

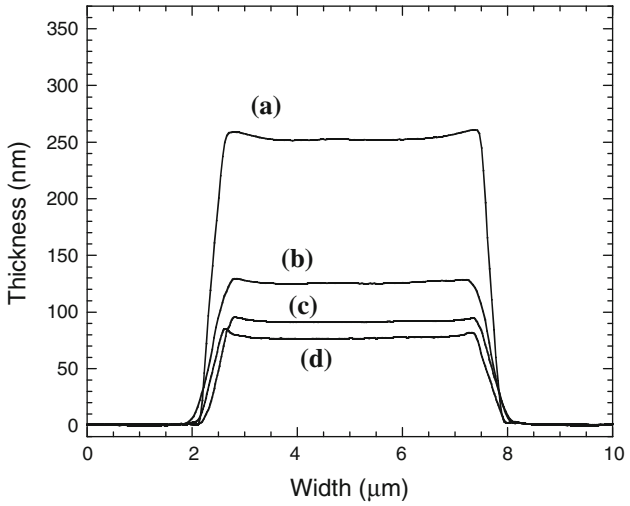

Fig. 10 AFM analysis of strip profiles formed through a 4/8-μm width/pitch mask on a gel film pre-dried for 2 h at 110 °C and submitted to post-patterning cumulative heat-treatments for 15 min at 200 (*a*), 300 (*b*), 400 (*c*), and 500 °C (*d*)

for the anatase phase). Images of Fig. 6b and c also demonstrate that a post-patterning heat-treatment at 500 °C does not degrade the strip width and height uniformity. A very weak RMS roughness value of 0.8 ± 0.05 nm was also measured on the patterned strips whatever the post-treatment temperature. These thermal features first indicate that opto-geometrical properties of photo-patterned structures can be adjusted in a very wide range, which allows envisaging efficient optimizations towards optical applications such as diffraction gratings [18].

A closer inspection of Figs. 6b, c, 9 and 10 shows that the pre-treatment duration induces some differences in profiles formed after post-treatments at various temperatures. Figure 10 indicates that, when the film has been pre-dried for a long duration, widths at the bottom and top of photo-patterned structures are not considerably modified when increasing the post-treatment temperature. In contrast, Fig. 9 shows that increasing this temperature causes a significant reduction of width at the top of structures formed after a short pre-drying treatment, and this reduction is again more marked at their bottom. The most striking feature illustrated in Figs. 6c and 9 is the formation of a multi-level sub-micrometric structure appearing on the edges of the photo-patterned surfaces in the case of films pre-dried for a short duration. Such a substructure, which is never or non-significantly observed when a long pre-drying treatment is performed (Figs. 6b, 10), appears after a heat-treatment at 200 °C and becomes more and more pronounced when increasing the heat-treatment temperature. After heating at 500 °C, Figs. 6c and 9 show that the height on the edges of photo-imprinted structures is about twice greater than at their centre. Some irregularities are also observed at the bottom of strips illustrated in Fig. 9. These irregularities are almost not perceptible for patterned structures heat-treated at low temperature and they appear more and more marked when increasing the heat-treatment temperature, i.e. when the height of substructures increases. Similar features were observed after selective laser writing and subsequent heat-treatments at high temperature, which indicated that the substructures did not depend on the choice of the photolithography method. Such a substructure has, as far as we are informed, never been described and discussed in the literature devoted to the photo-patterning of sol–gel oxide films.

Thermal stress effects: discussion

As illustrated in Figs. 4 and 5, the pre-drying treatment duration can induce some modifications in mechanisms occurring during the three-step photo-patterning procedure. Such modifications can in turn influence chemico-structural transformations taking place during a post-treatment at more or less high temperature. Successive transformations are expected to take place during such heat-treatment, including residual solvent evaporation, pyrolysis of remnant organic species, formation of an oxide network, and subsequent crystallization of this network. It is inferred that these chemico-structural transformations can in turn be influenced by the nature of residual species (butanol- or BzAc-derived species) present in the films after a more or less prolonged pre-drying period and subsequent UV exposure. Accordingly, we observed that films dried for a short duration underwent a delayed crystallization during

subsequent treatment at high temperature. This feature is illustrated in XRD patterns of Fig. 11 for films pre-dried at 110 °C and subsequently heat-treated for 15 min at 450 or 500 °C. After heat-treatment at 450 °C, the XRD pattern of a film pre-dried for 2 h at 110 °C exhibits distinct reflections of the crystalline TiO_2 anatase phase (Fig. 11a), according to ICDD card # 00-021-1272. In contrast, these reflections are absent in the pattern of a film pre-treated for 2 min at 110 °C and subsequently heat-treated at a same temperature of 450 °C (Fig. 11b). It indicates that a short heat-treatment of 15 min at 450 °C is not sufficient to induce crystallization after a short pre-drying step. For such pre-drying conditions, crystallization could be evidenced only after a heat-treatment at 500 °C (Fig. 11c). Thus, XRD data confirm that a short pre-drying step induces delayed chemico-structural transformations during subsequent heat-treatments at higher temperatures. The exact origin of features illustrated in Fig. 11 requires complementary studies. However, as discussed below, it is believed that such features can significantly influence the profile of photo-patterned structures heat-treated at more or less high temperature in relation to thermal stress effects.

First, in continuous (non-patterned) TiO_2 gel films submitted to a heat-treatment, several factors can cause the appearance of planar tensile or compressive stresses [27]. During an initial heating stage, planar stresses can develop owing to a differential thermal expansion at the film/substrate interface. However, it is inferred that during this rapid stage the relatively soft initial gel film can in part accommodate such stresses. Internal tensile stresses can then develop during the isothermal heat-treatment owing to aforementioned thermo-induced chemico-structural transformations. In the vertical direction, the film can efficiently relax these stresses through densification mechanisms. Owing to a strong attachment of the film to the substrate, this relaxation is not possible in the planar dimension, and the film undergoes internal planar tensile stresses. A rather stiff titanium oxide (amorphous or crystallized) film is also expected to be formed through chemico-structural transformation occurring during the isothermal treatment. Thus, external planar compressive stresses can then develop during the final cooling stage, owing to the stronger thermal expansion coefficient of the silicon substrate (2.6×10^{-6} °C^{-1}) compared to that of a TiO_2 film (0.32×10^{-6} °C^{-1}) [27]. To summarize, sol–gel films exposed to a heat-treatment undergo a complex competitive process between tensile and compressive planar stresses, which in turn depends on different experimental features (sol–gel formulations, heat-treatment conditions). As illustrated by XRD data of Fig. 11, it is inferred that films arising from a shorter pre-drying treatment undergo less complete chemico-structural transformation during the isothermal heat-treatment. Such films should thus undergo weaker tensile stresses during this isothermal treatment. Consequently, it is possible that the influence of compressive stresses developed during the final cooling stage predominates in such films when compared to films arising from a long pre-drying treatment.

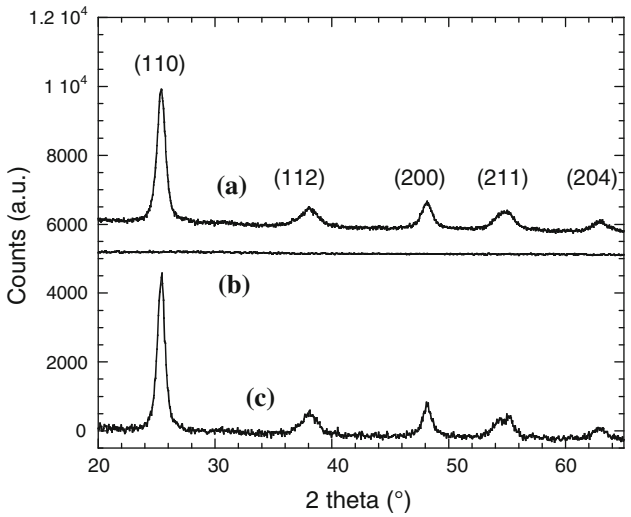

Fig. 11 XRD patterns of a film pre-dried for 2 h at 110 °C and subsequently heat-treated for 15 min at 450 °C (*a*), and for films pre-dried for 2 min at 110 °C and subsequently heat-treated for 15 min at 450 °C (*b*) and 500 °C (*c*). Reflections of the crystalline TiO_2 anatase phase are indexed

These arguments can then be extrapolated to photo-patterned structures. Owing to their 2-D profile, compared to a 1-D profile in the case of non-patterned films, these structures can undergo specific stress effects during thermal treatments. Indeed, planar stresses developed in continuous films are expected to be isotropically and uniformly distributed through the film surface while it has been shown that, in the case of an anisotropic structuration, such planar stresses can act in only one direction [28–31]. On the one hand, AFM profiles illustrated in Figs. 9 and 10 show that, owing to thermal stress relaxation, photo-patterned structures undergo thermo-induced densification effects yielding a marked thickness reduction, similarly to what is usually observed for continuous thin films. On the other hand, contrary to a continuous film where stress relaxation can only act in the vertical dimension, in patterned structures this relaxation can also act in the planar dimension. Such a planar relaxation seems to be illustrated at least for AFM profiles depicted in Fig. 9, which shows that increasing the post-treatment temperature induces a marked reduction of the photo-patterned structure widths. However, stress relaxation cannot wholly explain differences in profiles, as illustrated in Figs. 9 and 10. On the one hand, owing to a strong attachment of the photo-patterned structure to the substrate, width reduction induced by stress relaxation is expected to occur more efficiently at the top of

photo-patterned structures, and this relaxation cannot explain strong width reductions at the structure bottom, as illustrated in Fig. 9. On the other hand, we previously indicated that the influence of external compressive planar stresses can predominate in the case of films pre-dried for a short duration and subsequently heat-treated at more or less high temperature. Such compressive stresses may in turn explain the strong reduction of width at the bottom of photo-patterned structures, as illustrated in Fig. 9. Thus, these arguments suggest that profiles of structures formed through our photo-patterning procedure can undergo complex competitive processes between anisotropic tensile and compressive stresses when submitted at a more or less high temperature post-treatment, in relation to the pre-drying treatment duration. In this hypothesis, it is not excluded either that, in the case of a short pre-drying treatment, such a competitive process can favour the formation of substructures illustrated in Fig. 9 owing to the predominant influence of compressive planar stresses. In very different experimental conditions, other authors have also mentioned that anisotropic stresses can promote the formation of substructures at the surface of photo-imprinted patterns [28–31]. In the present state, it has not been established how such substructures can influence optical properties of photo-patterned films, for instance for diffraction grating applications, but it will be shown in the following section how this effect can interestingly influence some original surface properties.

Some examples of derived functionalities

Beside interests in optical applications, TiO_2-derived patterns can exhibit additional functionalities, which are exemplified in this section. In previous studies, we showed that a strong photocatalytic activity of TiO_2 films deposited from a pure sol 2 could arise from an optimization of structural and morphological features of such films, which relied on a post treatment in a 500–600 °C thermal range [32, 33]. In preliminary studies, we also verified that such strong photo-activity could be produced on TiO_2 films deposited from a mixed BzAc-derived sol (sol 1 + sol 2) and subsequently heat-treated at 500 °C (not illustrated here). Such a photo-activity can, for instance, be considered to induce a self-cleaning functionality at the surface of TiO_2 films thank to oxidative decomposition mechanisms induced by holes and electrons photo-generated in the film under UV light [1]. Such functionality may in turn have an added value when transposed to photo-patterned TiO_2 structures. Photo-activity features are punctually exemplified in this article by an original experiment. A TiO_2 film, patterned through a 2/4-μm width/pitch mask and crystallized at 500 °C, was then immersed within an $AgNO_3$ water–ethanol liquid solution and subsequently exposed to UV light for 1 h. More detailed data on this procedure have been presented in our previous article [34]. In this article, we showed that, in the case of non-patterned continuous TiO_2 films, such conditions promoted a photocatalytic reduction of adsorbed $AgNO_3$ species induced by electrons photo-generated in the film. This reduction rapidly yielded the formation of Ag° metal particles fixed at the TiO_2 film surface. Extrapolation of such a procedure to photo-patterned films is illustrated in the FEG-SEM image of Fig. 12. Owing to weight contrast effects, SEM images enable an unambiguous distinction between areas coated or not with silver particles. Bright areas observed in Fig. 12 depict the presence of Ag° metallic particles while darker areas correspond to the bare silicon substrate. It is clearly observed that silver particles form very homogeneous and linear strips whose width fairly respects that of the mask motifs, i.e. that of photo-patterned TiO_2 structures. Any Ag° particles, which would be evidenced by bright spots, cannot be detected on bare (TiO_2-free) silicon areas. This result shows that a photocatalytic metallization mechanism can efficiently be adapted to photo-patterned TiO_2 structures, which allows a localized control of Ag° particles at the substrate surface. The fine patterning of TiO_2 sol–gel films can, therefore, be extrapolated to a low-cost and very simplified photolithographic protocol adapted to metal structures, using a process entirely based on wet chemistry methods. For instance, such a protocol can impact applicative fields such as opto-electronics devices [35, 36], SERS substrates for organic probe applications [37–39], or wire-grid polarizers [40].

It is known that morphology features, such as roughness or surface porosity, can strongly increase the water contact angle of a naturally hydrophobic surface. This feature is accounted for by different theoretical models and

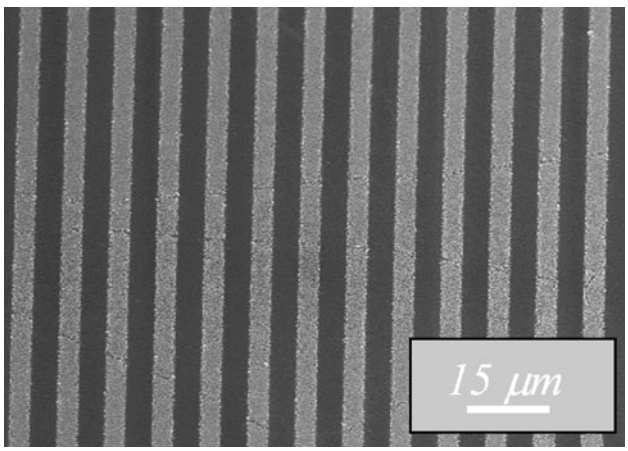

Fig. 12 FEG-SEM image of a TiO_2 film photo-patterned through a 2/4-μm width/pitch mask, heat-treated at 500 °C, and subsequently immersed within an $AgNO_3$ liquid solution and exposed to UV light for 1 h

can present different interests, including applications to water-repellent surfaces, anti-corrosion protections, or anti-bacterial functionalizations [41–46]. In a recent study, we have studied sol–gel-derived films deposited from a hexadecyltrimethoxysilane (C16) precursor [44]. The optimized insertion of long alkyl chains of this precursor in the oxide film induced a moderate hydrophobic behaviour characterized by a water contact angle of 105°. In another recent study, we have also shown that a TiO_2 surface presents a strong reactivity to sol–gel hetero-condensation reactions, which can be exploited to graft silicon alkoxide species through the formation of Ti–O–Si bonds [47]. In this study, we have taken advantage of these previous works to propose a simplified protocol yielding enhanced hydrophobic behaviours on photo-patterned TiO_2 structures. The C16 precursor was first diluted in absolute ethanol at various concentrations and so-formed solutions were then impregnated by spin-coating on TiO_2 patterns crystallized at 500 °C. After impregnation, the photo-patterned films were rinsed with ethanol to eliminate excess of C16 molecules non-grafted on the surface, dried with air spray, and finally heated for 10 min at 110 °C. For comparison purposes, non-patterned films heat-treated in similar conditions were also impregnated with C16 solutions of various concentrations. A maximal water contact angle of 105° was measured on these later films after impregnation of a 0.2-M C16 solution (not illustrated here). Such a maximal contact angle value has already been reported in our group [44] and also by others authors [48, 49] for silicon or glass planar supports impregnated with C16 species, i.e. in conditions where the substrate morphology cannot influence the surface wettability. It is thus believed that this contact angle value depicts an intrinsic hydrophobic behaviour of C16 species on a planar surface. In this study, such a value also suggests an efficient C16 grafting at the TiO_2 film surface using our simplified protocol based on Ti–O–Si hetero-condensation reactions (in contrast, non-grafted TiO_2 films exhibited a marked hydrophilic behaviour). Figure 13b illustrates the profile of a water droplet deposited on a photo-patterned film arising from a pre-drying treatment of 2 h. As shown in Fig. 10d, such conditions promoted the formation of patterned structures without substructure. A water contact angle of 120° is illustrated in Fig. 13b. Compared to that measured on planar surfaces, this larger contact angle suggests a synergy between the hydrophobic character induced by a C16 grafting and the micrometric structuration induced by our photo-patterning procedure. Figure 13a illustrates water contact angle variations as a function of the C16 concentration in ethanol for photo-patterned films arising from a pre-drying treatment of 2 min. As shown in Fig. 9d, such conditions promoted the formation of patterned structures with a sub-micrometric substructure. Data illustrated in

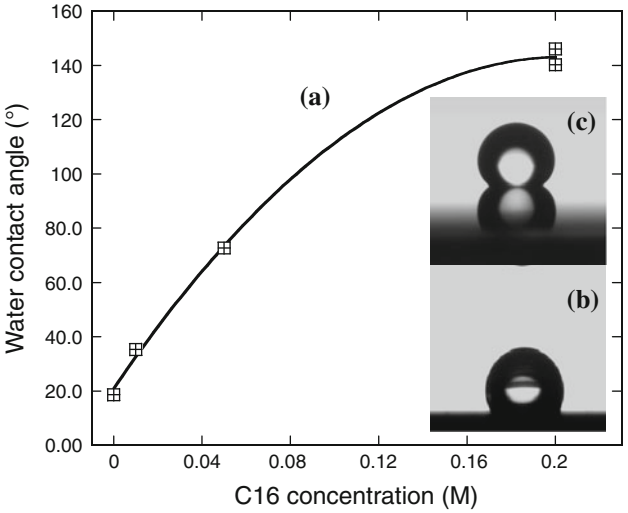

Fig. 13 Water contact angle variations versus C16 concentration in liquid solution for photo-patterned films pre-dried for 2 min at 110 °C, submitted to a post-patterning heat-treatment at 500 °C for 15 min, and finally grafted with C16 species (**a**). Water droplet profiles are illustrated in (**b**, **c**), for photo-patterned films pre-dried for 2 h and 2 min, respectively, before subsequent heat-treatment and impregnation within a 0.2-M C16 solution

Fig. 13a show that a variation of the C16 concentration in ethanol allows monitoring the surface properties from a hydrophilic to a strongly marked hydrophobic behaviour. As illustrated in Fig. 13c, a water contact angle of 145° is measured after impregnation from a 0.2-M C16 solution on such photo-patterned structures. Compared to that illustrated in Fig. 13b, this much larger value suggests an enhanced synergy between a natural hydrophobic functionalization and a multi-level surface roughness effects, according to mechanisms previously proposed by other authors [46]. These data illustrate a very simplified protocol to form strongly hydrophobic surfaces. It is even supposed that such surface properties may again be enhanced through an optimization of photo-patterning conditions, which will be the object of further studies.

Conclusion

Homogeneous microstructure patterns have been directly photo-imprinted on sol–gel-derived TiO_2 films through photolithographic mask transfer or laser writing methods using UVA light. For that purpose, specific BzAc-derived sol–gel formulations were set-up, which associated two sols of strongly different reactivities. Then a three-step photo-patterning protocol was adopted. These experimental conditions finally promoted enhanced solubility contrasts between irradiated and non-irradiated areas. Though additional studies are still required to reduce the duration of UV exposure through a mask or increase the laser writing

speed, promising results have already been obtained. It has first been shown that, while a pre-drying treatment performed before UVA irradiation does not significantly modify the homogeneity of resulting patterns, it can strongly influence their profile shape. On the one hand, microstructures arising from a long pre-drying treatment exhibit a regular shape (width and height), whatever the temperature of a post-patterning heat-treatment. On the other hand, a multilevel sub-micrometric structure is formed on patterns arising from a short pre-drying treatment and heated at 200 °C or more after photo-patterning. It is believed that a complex combination of anisotropic thermal stresses induced by the heat-treatment can favour such a substructure. It has also been shown that the heat-treatment allows monitoring the thickness and refractive index values of TiO_2 samples in a wide range of values. Above 450 °C, the heat-treatment also promotes the crystallization of BzAc-derived films, which in turn confers a good photocatalytic activity to photo-patterned TiO_2 structures. This activity has in particular been exploited to propose a very simplified lithography protocol adapted to the localized deposition of metal silver particles, which is based on a photocatalytic reduction mechanism at the surface of photo-patterned TiO_2 films. Finally, while TiO_2-derived patterns can present interests in optical applications, such as diffraction gratings, we have also shown that a synergy between a photo-induced structuration and the efficient grafting of a C16 precursor yields an easy way to form surfaces with enhanced hydrophobic properties.

References

1. Carp O, Huisman CL, Reller A (2004) Prog Solid State Chem 32:33
2. Langlet M (2005) In: Sakka S (ed) Sol–gel processing. Kluwer, Norwell, p 1
3. Cotton DV, Fell CJ, Dastoor PC (2009) Synth Met 159:456
4. Gonsalves KE, Wang M, Lee CT, Yueh W, Tapia-Tapia M, Batina N, Henderson CL (2009) J Mater Chem 19:2797
5. Im SG, Kim BS, Tenhaeff WE, Hammond PT, Gleason KK (2009) Thin Solid Films 517:3606
6. Soppera O, Jradi S, Lougnot DJ (2008) J Polym Sci A 46:3783
7. El Ahrach H, Bachelot R, Vial A, Lerondel G, Plain J, Royer P, Soppera O (2007) Phys Rev Lett 98:107402
8. Cai Y, Ocko B (2005) J Am Chem Soc 127:16287
9. Christman KL, Schopf E, Broyer RM, Li RC, Chen Y, Maynard HD (2009) J Am Chem Soc 131:521
10. Seo K, Borguet E (2006) Langmuir 22:1388
11. Lee WK, Whitman LJ, Lee J, King WP, Sheehan PE (2008) Soft Matter 4:1844
12. Huh JW et al (2009) Appl Phys Lett 94:223311
13. Graeter SV, Huang J, Perschmann N, Lopez-Garcia M, Kessler H, Ding J, Spatz JP (2007) Nano Lett 7:1413
14. Yoon B, Acharya H, Lee G, Kim H-C, Huh J, Park C (2008) Soft Matter 4:1467
15. He X, Winkel J, Huck WT (2009) Adv Mater 21:2083
16. Jegadesan S, Sindhu S, Advincula RC, Valiyaveettil S (2006) Langmuir 22:780
17. Ridaoui H, Wieder F, Ponche A, Soppera O (2010) Nanotechnology 21(1–10):065303
18. Tohge N, Zhao G, Chiba F (1999) Thin Solid Films 351:85
19. Saifullah MSM, Subramanian KRV, Tapley E, Kang DJ, Welland ME, Butler M (2003) Nano Lett 3:1587
20. Tohge N, Shinmou K, Minami T (1994) Sol-Gel Opt III 2288:589
21. Imao T, Hazama D, Noma N, Ito S (2006) J Ceram Soc Jpn 114:238
22. Langlet M, Burgos M, Coutier C, Jimenez C, Morant C, Manso M (2001) J Sol-Gel Sci Technol 22:139
23. Burgos M, Langlet M (1999) Thin Solid Films 341(1–2):19
24. Araña J, Doña-Rodrıguez JM, Garriga i Cabo C, González-Dıaz O, Herrera-Melián JA, Pérez-Peña J (2004) Appl Catal B 53:221
25. Millon C, Riassetto D, Berthomé G, Roussel F, Langlet M (2007) J Photochem Photobiol A 189:334
26. Briche S, Riassetto D, Gastaldin C, Lamarle C, Dellea O, Jamon D, Pernot E, Labeau M, Ravel G, Langlet M (2008) J Mater Sci 43:5809. doi:10.1007/s10853-008-2884-7
27. Rabaste S, Bellessa J, Brioude A, Bovier C, Plenet JC, Brenier R, Marty O, Mugnier J, Dumas J (2002) Thin Solid Films 416:242
28. Yoo PJ, Suh KY, Park SY, Lee HH (2002) Adv Mater 14:1383
29. Takahashi M, Maeda T, Uemura K, Yao J, Tokuda Y, Yoko T, Kaji H, Marcelli A, Innocenzi P (2007) Adv Mater 19:4343
30. Bowden N, Brittain S, Evans AG, Hutchinson JW, Whitesides GM (1998) Nature 393:146
31. Takahashi M, Uemura K, Maeda T, Yao J, Tokuda Y, Yoko T, Costacurta S, Malfatti L, Innocenzi P (2008) J Sol-Gel Sci Technol 48:182
32. Fallet M, Permpoon S, Deschanvres JL, Langlet M (2006) J Mater Sci 41(10):2915. doi:10.1007/s10853-006-5077-2
33. Langlet M, Permpoon S, Riassetto D, Berthomé G, Pernot E, Joud JC (2006) J Photochem Photobiol A 181(2–3):203
34. Riassetto D, Roussel F, Rapenne L, Roussel H, Chaix O, Micoud F, Chatenet M, Langlet M (2010) J Exp Nanosci 5(3):221
35. Cozzoli PD, Fanizza E, Comparelli R, Curri ML, Agostiano A, Laub D (2004) J Phys Chem B 108:9623
36. Kim KD, Han DN, Lee JB, Kim HT (2006) Scr Mater 54:143
37. Chou PW, Treschev S, Chung PH, Cheng CL, Tseng YH, Chen JY, Wong MS (2006) Appl Phys Lett 89(1–3):131919
38. Norrod KL, Sudnik LM, Rousell D, Rowlen KL (1997) Appl Spectrosc 51:994
39. Li X, Xu W, Jia H, Wang X, Zhao B, Li B, Ozaki Y (2004) Appl Spectrosc 58:26
40. Ahn SH, Kim JS, Guo LJ, Vac (2007) J Sci Technol B 25(6):2388
41. Hoefnagels HF, Wu D, De With G, Ming W (2007) Langmuir 23:13158
42. Xue CH, Jia ST, Chen HZ, Wang M (2008) Sci Technol Adv Mater 9:035001
43. Xue CH, Jia ST, Zhang J, Tian LQ, Chen HZ, Wang M (2008) Sci Technol Adv Mater 9:035008
44. Houmard M, Vasconcelos DCL, Vasconcelos WL, Berthomé G, Joud JC, Langlet M (2009) Surf Sci 603:2698
45. Osawa S, Yabe M, Miyamura M, Mizuno K (2006) Polymer 47:3711
46. Ming W, Wu D, Van Benthem R, De With G (2005) Nano Lett 5:2298
47. Houmard M, Riassetto D, Roussel F, Bourgeois A, Berthomé G, Joud JC, Langlet M (2007) Appl Surf Sci 254:1405
48. Mahltig B, Haufe H, Bottcher H (2005) J Mater Chem 15:4385
49. Mahltig B, Bottcher H (2003) J Sol-Gel Sci Technol 27:43